



HAL
open science

Automatized set-up procedure for transcranial magnetic stimulation protocols

Sylvain Harquel, Julien Diard, Estelle Raffin, Passera Brice, Dall'Igna Gaelle, Christian Marendaz, Olivier David, Alan Chauvin

► To cite this version:

Sylvain Harquel, Julien Diard, Estelle Raffin, Passera Brice, Dall'Igna Gaelle, et al.. Automatized set-up procedure for transcranial magnetic stimulation protocols. *NeuroImage*, 2017, Epub ahead of print. 10.1016/j.neuroimage.2017.04.001 . inserm-01504574

HAL Id: inserm-01504574

<https://inserm.hal.science/inserm-01504574>

Submitted on 10 Apr 2017

HAL is a multi-disciplinary open access archive for the deposit and dissemination of scientific research documents, whether they are published or not. The documents may come from teaching and research institutions in France or abroad, or from public or private research centers.

L'archive ouverte pluridisciplinaire **HAL**, est destinée au dépôt et à la diffusion de documents scientifiques de niveau recherche, publiés ou non, émanant des établissements d'enseignement et de recherche français ou étrangers, des laboratoires publics ou privés.

Public Domain

Automatized set-up procedure for transcranial magnetic stimulation protocols

S. Harquel^{a,b,c,d,*}, J. Diard^{a,b}, E. Raffin^{a,c}, B. Passera^{a,b}, G. Dall’Igna^{e,c}, C. Marendaz^{a,b}, O. David^{a,c}, A. Chauvin^{a,b}

^a*Univ. Grenoble Alpes, F-38000 Grenoble, France*

^b*CNRS, UMR 5105, Laboratoire de Psychologie et de Neurocognition, LPNC, F-38000 Grenoble, France*

^c*INSERM, U1216, Grenoble Institut des Neurosciences, GIN, F-38000 Grenoble, France*

^d*CNRS, INSERM, UMS 3552, IRMaGe, F-38000 Grenoble, France*

^e*Pôle de Psychiatrie et Neurologie, Centre Hospitalier Universitaire Grenoble Alpes, F-38000 Grenoble, France*

Abstract

Transcranial Magnetic Stimulation (TMS) established itself as a powerful technique for probing and treating the human brain. Major technological evolutions, such as neuronavigation and robotized systems, have continuously increased the spatial reliability and reproducibility of TMS, by minimizing the influence of human and experimental factors. However, there is still a lack of efficient set-up procedure, which prevents the automation of TMS protocols. For example, the set-up procedure for defining the stimulation intensity specific to each subject is classically done manually by experienced practitioners, by assessing the motor cortical excitability level over the motor hotspot (HS) of a targeted muscle. This is time-consuming and introduces experimental variability. Therefore, we developed a probabilistic Bayesian model (AutoHS) that automatically identifies the HS position. Using virtual and real experiments, we compared the efficacy of the manual and automated procedures. AutoHS appeared to be more reproducible, faster, and at least as reliable as classical manual procedures. By combining AutoHS with robotized TMS and automated motor threshold estimation methods, our approach constitutes the first fully automated set-up procedure for TMS protocols. The use of this procedure decreases inter-experimenter variability while facilitating the handling of TMS protocols used for research and clinical routine.

Keywords: robotized TMS, hotspot hunting, cortical excitability, MEP, motor mapping

Highlights

- Automatized set-up procedures would facilitate TMS experiments and increase reproducibility
- We developed a Bayesian model aiming at automatically finding the motor hotspot
- Implementation of this model in a robotized TMS system allows the automatic search for the motor hotspot
- Definition of the motor hotspot is significantly improved in terms of speed and reproducibility

*Corresponding author. Laboratoire de Psychologie et de Neurocognition, CNRS UMR 5105. Université Grenoble Alpes, BSHM. BP47, 38040 Grenoble Cedex 9, France. Tel: +334 76 82 58 91. Mail: sylvain.harquel@univ-grenoble-alpes.fr. Webpage: <http://lpnc.univ-grenoble-alpes.fr/Sylvain-Harquel?lang=fr>

1. Introduction

Transcranial Magnetic Stimulation (TMS) is a non-invasive brain stimulation technique (Barker et al., 1985 ; Hallett, 2000). Applied alone or coupled with other neuroimaging techniques (Bestmann and Feredoes, 2013), its application are now numerous in both fundamental (Rogasch and Fitzgerald, 2013 ; Bortoletto et al., 2015) and clinical research (Ragazzoni et al., 2013 ; Lefaucheur et al., 2014 ; Lefaucheur and Picht, 2016).

In order to standardize procedures and consequently reduce inter-subject variability in response to TMS, the field has recently embraced major technological evolutions. Neuronavigation systems dedicated to TMS (Herwig et al., 2001) significantly improved its spatial precision and reproducibility (Julkunen et al., 2009 ; Weiss et al., 2013) and TMS-robotized systems enabled the automation of coil positioning (Finke et al., 2008 ; Kantelhardt et al., 2009 ; Ginhoux et al., 2013). In addition to improving spatial precision and reproducibility compared to manual positioning (Ginhoux et al., 2013), robotized TMS paves the way for new acquisition protocols, such as automated cortical mapping procedures (Harquel et al., 2016a). It is thus likely that the future of TMS resides in the full automation of protocols, partly enabled by robotics.

Every TMS protocol begins by a mandatory set-up procedure, which aims at defining the stimulation intensity to be employed on the cortical target (Rossi et al., 2009 ; Herbsman et al., 2009 ; Wassermann and Epstein, 2012). This intensity has to be defined specifically for each subject because it depends on individual neuroanatomy. The procedure consists in assessing the resting (or active) motor threshold (rMT, or aMT) by measuring the muscular activity evoked by the stimulation of the motor hotspot (HS) over the primary motor cortex (M1). Stimulation intensities are then most often expressed as a percentage of this threshold, in order to conform to safety guidances and to standardize stimulation power between subjects (Herbsman et al., 2009).

Depending on its definitions (Meincke et al., 2016), the HS corresponds to the cortical target over M1 where TMS evokes the lowest MT (Rossini et al., 1994), or the largest motor evoked potentials (MEPs) on the targeted muscle (van de Ruit et al., 2015). While efficient automated MT estimation methods have already been developed and are used since then (Awiszus, 2003 ; Awiszus and Borckardt, 2011), it is not the case for HS hunting. In practice, the HS position is manually set by experienced practitioners, even though Meincke et al. (2016) recently developed the first automated HS hunting procedure using the mapping of MTs. This method appeared to be effective in automatically assessing the HS position, and producing insightful data for motor mapping protocols. However, its substantial duration (over one hour) prevents its practical use in clinical settings and in most TMS experiments. Although quicker (about ten minutes),

32 manual set-up procedures also have limitations: i. they represent an additional source of inter-experimenter
33 variability (Gugino et al., 2001 ; Cincotta et al., 2010 ; Sollmann et al., 2013), ii. they require well-trained
34 TMS practitioners, and iii. they rely on the observation of MEP mean amplitudes which are highly variable
35 (Wassermann, 2002 ; Jung et al., 2010).

36 In order to overcome these limitations, we propose here an automated HS hunting procedure (AutoHS)
37 based on a Bayesian model. AutoHS aims at localizing the HS in a faster, more reliable and more reproducible
38 way compared to a manual HS hunting performed by TMS experimenters. The present paper describes how
39 we implemented HS hunting in a Bayesian model, and how we tested our method on virtual data and
40 validated it against manual HS hunting performed by four TMS experts on 19 healthy volunteers. We
41 finally discuss our method and its relevance for progressing towards fully automated set-up procedures for
42 TMS protocols.

43 **2. Materials & Methods**

44 We describe first the Bayesian model of AutoHS in detail and second the experimental procedure used
45 to test and compare AutoHS to manual methodology. Throughout this work, the targeted muscle for the
46 HS hunting procedure is the first interosseous muscle (FDI).

47 *2.1. Bayesian model of AutoHS*

48 *2.1.1. Overview*

49 AutoHS is a probabilistic procedure, as is classical in the domain of multisensor data fusion in robotics
50 (Bessière and Lebeltel, 2008). Its objective is to estimate the HS position, using the history of stimulated
51 sites and recorded MEP amplitudes.

52 AutoHS is built in two steps, applying the Bayesian programming methodology (Bessière et al., 2013).
53 The first step consists in defining the joint probability distribution over five variables, including the HS
54 position. From this joint probability distribution, the second step consists in applying Bayesian inference,
55 so as to compute the probability distribution over HS positions, conditioned on previous observations. This
56 procedure is complemented by a “smart” prospective method, that considers the most promising next cortical
57 position to be stimulated, in terms of information gain (Baek et al., 2016), in order to find the HS as fast
58 as possible. AutoHS automatically stops and settles on the HS position once enough information has been
59 gathered.

60 The method was implemented using Matlab (The Mathworks Inc., USA) and was run concurrently with
61 the neuronavigation and the EMG recording systems. The default values of the model variables used in this

62 work are reported throughout this section. These values have been estimated during pre-tests conducted on
 63 real motor mapping datasets not shown in this report. Their robustness are discussed later (see Discussion).

64 2.1.2. Model description

65 The structure of the Bayesian model is defined by specifying the joint probability distribution over the
 66 five following variables.

67 HS represents the spatial position of the HS. The model makes the assumption that the 3D stimulation
 68 space can be projected to a 2D stimulation grid placed on the scalp surface over the motor cortex
 69 (Figure 1a). HS is thus a two dimensional variable expressed in a Cartesian coordinate system. Its x
 70 and y values are continuous over the stimulation grid area, so that $(x_{HS}, y_{HS}) \in ([1; N_x], [1; N_y])$, with
 71 N_x and N_y being the number of discrete points in the stimulation grid. This work uses a square grid,
 72 so that $N_x = N_y = 7$. The spacing between points is set to 7 mm, leading to a 4.2 cm sided square.
 73 This spacing affords a good spatial resolution regarding cortical mapping, while still making sure to
 74 be twice above navigation precision (around 3 mm, including camera measurement uncertainty and
 75 MRI registration error).

76 AutoHS makes the initial assumption that the FDI HS is located on the hand knob of the precentral
 77 gyrus (primary motor cortex, M1). The prior probability distribution of HS over the stimulation space
 78 is thus a 2D-Gaussian distribution centered on this location:

$$P(HS) \propto \exp\left(-\left(\frac{(x - x_{HK})^2}{2\sigma_{prior}^2} + \frac{(y - y_{HK})^2}{2\sigma_{prior}^2}\right)\right), \quad (1)$$

79 where x_{HK} and y_{HK} are the coordinates of the hand knob, and σ_{prior} is the spatial spread of the
 80 distribution that quantifies the prior precision (Figure 1b). We use here $\sigma_{prior} = 2$ (in grid units),
 81 leading to a spatial spread of 1.4 cm.

82 S_i is the position of the coil at the i^{th} stimulation, i going from 1 to the total number of stimulated
 83 positions T . S_i is also a two dimensional variable expressed in a Cartesian coordinate system. How-
 84 ever, its x and y values are discrete and correspond to the nodes of the stimulation grid, so that
 85 $(x_i, y_i) \in (\{1, 2, \dots, N_x\}, \{1, 2, \dots, N_y\})$.

86 μ_i is the mean amplitude observed from N MEPs on S_i . μ_i is a discrete variable over the domain of possible
 87 MEP amplitudes D_{MEP} (in μV). Here, we set $D_{MEP} = \{10, 20, \dots, 4000\} \mu V$.

Here, μ_i is meant to follow a Gaussian distribution such that

$$P(\mu_i) \propto \frac{1}{\sigma_i \sqrt{2\pi}} \exp\left(-\frac{(\mu - \mu_i)^2}{\sigma_i^2}\right), \quad (2)$$

where σ_i is the standard deviation measured over the N recorded MEP amplitudes (Figure 1c). This work uses 5 MEP recordings per stimulation point, so that $N = 5$. If no MEP was induced after 3 consecutive stimulations, μ_i was set to 0 and the model moved to the next iteration.

μ_{HS} represents the expected mean amplitude measured on the HS. Here, in accordance with the HS definition (see 1), AutoHS makes the assumption that μ_{HS} represents the maximal mean MEP amplitude that can be measured over the whole simulation space. μ_{HS} is a discrete variable over the domain of possible MEP max amplitudes D_{max} (in μV). Here, we set $D_{max} = \{250, 500, \dots, 4000\} \mu\text{V}$.

Moreover, the model assumes that MEP amplitudes μ_i decrease as a function of the distance between the stimulated position S_i and the HS position HS (Figure 1d):

$$\mu_i = \mu_{HS} \exp\left(-\left(\frac{(x_i - x_{HS})^2}{2\sigma_{sp}^2} + \frac{(y_i - y_{HS})^2}{2\sigma_{sp}^2}\right)\right). \quad (3)$$

σ_{sp} is the standard deviation parameter of the 2D Gaussian pattern for MEP amplitude modulation (Eq. (3)). It represents the spatial spread of the muscle representation on the stimulation grid (Figure 1d). σ_{sp} is a discrete variable over the domain of possible muscle representation sizes D_{sp} (in grid units). Here, we set $D_{sp} = \{0.2, 0.4, \dots, 2\}$.

The joint probability distribution over the five above variables is then defined as follows:

$$P(HS \ \mu_{HS} \ \sigma_{sp} \ S_{1:T} \ \mu_{1:T}), \quad (4)$$

where $S_{1:T}$ and $\mu_{1:T}$ denotes the series of variables S_i and μ_i from the first to the last stimulated position.

The joint probability distribution is simplified, by the appropriate conditional hypotheses assumptions, in order to obtain a product of simpler probability distributions:

$$P(HS \ \mu_{HS} \ \sigma_{sp} \ S_{1:T} \ \mu_{1:T}) = P(HS) P(\mu_{HS}) P(\sigma_{sp}) \prod_{i=1}^T P(S_{1:T}) \prod_{i=1}^T P(\mu_i | A), \quad (5)$$

where A , for notational simplicity, is the conjunction of variables HS , μ_{HS} , σ_{sp} and S_i . The priors on μ_{HS} and σ_{sp} are kept uninformative because of high inter-subject variability regarding these values. $P(\mu_{HS})$

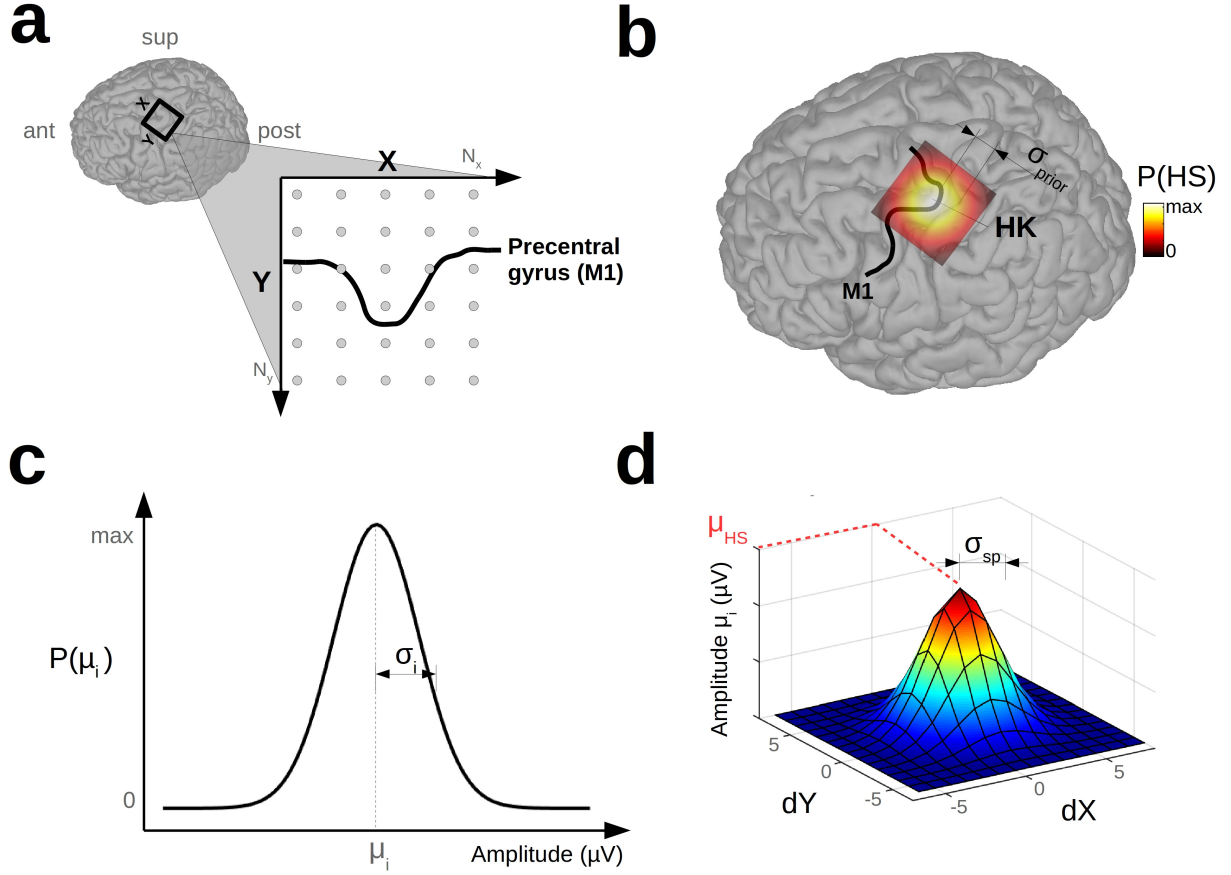


Figure 1: Main components and hypotheses of the AutoHS model. a: stimulation grid used for hunting and for expressing point coordinates. b: Probabilistic prior concerning HS position, centered on the hand knob of the primary motor cortex M1 (precentral gyrus). c: Probability distribution of MEP amplitudes, estimated on N EMG recordings. d: MEP mean amplitude (μ_i) modulation as a function of the distances dX and dY between S_i and HS along the X and Y-axis respectively.

108 and $P(\sigma_{sp})$ thus are uniform distributions over their respective domains. The prior on the stimulation
 109 position S_i is a Dirac distribution centered on the position selected during the previous iteration (see 2.1.5).
 110 S_1 is initialized on the center of the stimulation grid. Finally, $P(\mu_i | A)$ corresponds to the probability
 111 of measuring the MEP mean amplitude μ_i given the coordinates of the stimulated site S_i and HS , the
 112 estimated maximal amplitude μ_{HS} and spatial spread σ_{sp} of the muscle representation. We can write our
 113 knowledge μ_i given A in $P(\mu_i | A)$, by merging Eq. (2) and (3), so that:

$$\begin{aligned}
 P(\mu_i | A) &\propto \frac{1}{\sigma_i \sqrt{2\pi}} \exp\left(-\frac{(\mu - \mu_i)^2}{\sigma_i^2}\right) \\
 &\propto \frac{1}{\sigma_i \sqrt{2\pi}} \exp\left(-\frac{\left(\mu - \mu_{HS} \exp\left(-\left(\frac{(x_i - x_{HS})^2}{2\sigma_{sp}^2} + \frac{(y_i - y_{HS})^2}{2\sigma_{sp}^2}\right)\right)\right)^2}{\sigma_i^2}\right).
 \end{aligned} \tag{6}$$

114 *2.1.3. Question and inference*

115 The objective of AutoHS is to estimate the position of the HS, given all the MEP mean amplitudes $\mu_{1:T}$
 116 observed after stimulating cortical positions $S_{1:T}$. However, this is not possible without jointly inferring
 117 μ_{HS} and σ_{sp} , since these variables are also conditioning the probability $P(\mu_i | A)$. Therefore, the joint
 118 probability $P(HS \ \mu_{HS} \ \sigma_{sp} | \mu_{1:T} \ S_{1:T})$ is computed, which is a four-dimensional probability distribution.
 119 Bayesian inference yields (see appendix for the complete derivation):

$$P(HS \ \mu_{HS} \ \sigma_{sp} | S_{1:T} \ \mu_{1:T}) \propto P(HS) \prod_{i=1}^T P(\mu_i | A). \quad (7)$$

120 Once this distribution is evaluated, we compute its center of gravity, and the estimates for the HS x and y
 121 dimensions are its first two coordinates.

122 Because $P(HS \ \mu_{HS} \ \sigma_{sp} | \mu_{1:T} \ S_{1:T})$ is four dimensional, it is not easily displayed. For visualization, we
 123 thus compute and show the marginal distributions over each variable, that can be derived from Eq. (7):

$$\begin{aligned} P(HS | \mu_{HS} \ \sigma_{sp} \ S_{1:T} \ \mu_{1:T}) &\propto P(HS) \sum_{\mu_{HS}} \sum_{\sigma_{sp}} \prod_{i=1}^T P(\mu_i | A) \\ P(\mu_{HS} | HS \ \sigma_{sp} \ S_{1:T} \ \mu_{1:T}) &\propto P(HS) \sum_{HS} \sum_{\sigma_{sp}} \prod_{i=1}^T P(\mu_i | A) \\ P(\sigma_{sp} | \mu_{HS} \ HS \ S_{1:T} \ \mu_{1:T}) &\propto P(HS) \sum_{\mu_{HS}} \sum_{HS} \prod_{i=1}^T P(\mu_i | A) \end{aligned} \quad (8)$$

124 *2.1.4. Stop criteria*

125 If the inference on HS can be done after each stimulation i , the total number of stimulations T is *a priori*
 126 unknown, and depends on the information gained during the whole process. The level of information at the
 127 i^{th} iteration is assessed through the entropy h_i of the joint distribution inferred in Eq. (7):

$$h_i = - \sum_{HS} \sum_{\mu_{HS}} \sum_{\sigma_{sp}} P(HS \ \mu_{HS} \ \sigma_{sp} | S_{1:i} \ \mu_{1:i}) \ln(P(HS \ \mu_{HS} \ \sigma_{sp} | S_{1:i} \ \mu_{1:i})). \quad (9)$$

128 By definition, the entropy h_i starts at its theoretical maximum h_{max} and decreases throughout the HS
 129 hunting process as the model gains information. An increase of entropy during the process would incidentally
 130 reveal the violation of at least one of the model hypothesis.

131 A first stop criterion can then be set up by defining a threshold level to be reached by h_i . This threshold

132 is expressed as a proportion of h_{max} . The process thus stops after the i^{th} iteration whenever:

$$h_i < \alpha h_{max}, \quad (10)$$

133 with $\alpha \in (0; 1)$.

134 However, the situation where h_i never reaches this threshold also has to be considered. The occurrence
 135 of this bad-case scenario depends on the match between the recorded data and the model hypothesis, as well
 136 as on the variability of the data (σ_i). The second stop criterion is thus based on the first derivative dh_i/di .
 137 The process stops whenever the model does not get any further information from the data, i.e.:

$$\frac{dh_i}{di} < \beta, \quad (11)$$

138 where β is a real number close to 0. To prevent false-alarms, i.e. temporary decreases of information gain,
 139 the criterion has to be satisfied on two consecutive iterations. The default values used in this work are
 140 $\alpha = 0.3$ and $\beta = 0.2$.

141 2.1.5. Smart planning of S_{i+1}

142 AutoHS integrates a smart selection of the next stimulation position S_{i+1} . Although any procedure of
 143 position selection within the stimulation grid would be possible, a prospective choice of S_{i+1} allows the
 144 model to converge more rapidly to the HS.

145 To do so, the model estimates future entropy resulting from the virtual stimulation of each position:

$$\forall S_{i+1} \mid (x_{i+1}, y_{i+1}) \in (\{1, \dots, N_x\}, \{1, \dots, N_y\}),$$

146

$$h_{i+1} = - \sum_{HS} \sum_{\mu_{HS}} \sum_{\sigma_{sp}} P(HS \ \mu_{HS} \ \sigma_{sp} \mid S_{1:i+1} \ \mu_{1:i+1}) \ln(P(HS \ \mu_{HS} \ \sigma_{sp} \mid S_{1:i+1} \ \mu_{1:i+1})), \quad (12)$$

147 where μ_{i+1} is directly estimated using Eq. (3) and the current knowledge at iteration i about HS , μ_{HS}
 148 and σ_{sp} , and σ_{i+1} is equal to σ_i . AutoHS finally chooses the cortical position S_{i+1} inducing the maximal
 149 entropy decrease between iterations i and $i + 1$:

$$S_{i+1} \mid \max_{S_{i+1}}(h_i - h_{i+1}). \quad (13)$$

150 In order to avoid intensive stimulation over the same cortical positions, each point of the grid was limited to
151 two non-consecutive iterations during the whole hunting procedure. The model selected the point leading
152 to the next best entropy decrease in case of conflict with the previous rule.

153 *2.2. Experimental procedure*

154 *2.2.1. Subjects*

155 Nineteen right-handed healthy volunteers (14 males, aged 29.6 ± 10.1 years old) participated in the
156 protocol. They all gave their informed and written consent prior to the experiment and received payment
157 for their participation. None of them had either history of psychiatric or neurological disorders, or history
158 of alcohol or substance abuse. They were free of any medicinal treatment likely to modulate their motor
159 cortical excitability levels. MRI and TMS acquisitions were performed at IRMaGe MRI and Neurophysiology
160 facilities (Grenoble, France). The ethical committee of Grenoble University Hospital (ID RCB: 2013-A01734-
161 41) approved this study, which has been registered on ClinicalTrials.gov (number NCT02168413).

162 *2.2.2. Protocol design*

163 Subjects went through two stimulation sessions, separated by a delay of one week. Each session consisted
164 of the two tested TMS set-up procedures: manual and automatized. The order of the procedures was
165 counterbalanced between subjects and sessions. Each procedure consisted in one hotspot-hunting step
166 followed by a resting motor threshold (rMT) assessment. Ten baseline MEPs were also recorded using an
167 intensity of 120% rMT, in order to assess the influence of the procedures on its variability. In one of the two
168 sessions, an extensive motor mapping was done either before, between or after the two procedures.

169 *2.2.3. Anatomical MRI processing*

170 Prior to the stimulation sessions, a cerebral anatomical T1-weighted MRI was acquired at 3T (Achieva
171 3.0T TX, Philips, Netherlands) for each subject. The MRI data were entered in the TMS neuronavigation
172 system (Localite GmbH, Germany) for post-processing. First, the anatomical hotspot (HS_{anat}) for the
173 right FDI muscle was defined according to its classical location in the hand knob of the left precentral gyrus
174 (primary motor cortex) (Yousry et al., 1997). Second, a grid of stimulation positions was defined as a square
175 of seven by seven points centered on HS_{anat} and oriented with respect to the central sulcus (Figure 1a).
176 This grid was automatically generated on the 3D segmented cortex using the dedicated function of the
177 neuronavigation software. The distance between points on the cortical surface was set to 7 mm, resulting in
178 a 17.64 cm^2 stimulation area. The X-axis was in the lateral-medial direction, its origin being at the most

179 lateral point, while the Y-axis ranged from the most anterior point to the most posterior one. All spatial
180 coordinates reported throughout this manuscript were projected to and expressed in this 2D-Cartesian
181 coordinate system.

182 2.2.4. Manual set-up procedure

183 The manual set-up procedure (mSUP) was performed by an experienced TMS practitioner. Four local
184 experimenters (three neurophysiologists and one psychiatrist) participated in this study. They were ran-
185 domly distributed and counterbalanced between subjects and sessions, so that they never processed the
186 same subject twice. The experimenters were blind to the other set-up procedures.

187 In order to reduce inter-experimenter variability, normalized guidelines were followed throughout the
188 experiment. First, the HS hunting session had to start on HS_{anat} using an *a priori* stimulation intensity
189 of 55 % of the maximal stimulator output. A minimum of three MEPs had to be recorded on each tested
190 stimulation point. The experimenters were free to increase or decrease the stimulation power during HS
191 hunting. Finally, they were asked to continuously control the coil angles so that the coil was tangential to
192 the scalp surface and the stimulation angle was perpendicular to the central sulcus. Once experimenters
193 considered they found the HS position, they were asked to maintain the coil in its position during rMT and
194 baseline measurements using the neuronavigation marker.

195 2.2.5. Automatized set-up procedure

196 The automatized set-up procedure (aSUP) was completed by the robotized TMS system together with
197 AutoHS (Figure 2). The procedure began with an initial threshold rMT_{anat} estimated on HS_{anat} . HS
198 hunting then started on HS_{anat} , using an exploration intensity I of 110% of rMT_{anat} . Since the measured
199 rMT increases while moving away from the HS, this intensity always ensured a supraliminal stimulation
200 level while preventing from stimulating too much, in the case where HS_{anat} was too far from the actual
201 HS position. On each stimulated position, five MEP amplitudes (see 2.1) were recorded and entered into
202 AutoHS. Upon computation completion, AutoHS provided the next cortical position to be stimulated. This
203 position was then manually selected in the neuronavigation system (see 2.2.7), in order to put the robotized
204 coil on it. Once over the HS position defined by AutoHS, the robot maintained the coil on it during rMT
205 and baseline measurements.

206 2.2.6. Motor mapping

207 An extensive motor mapping procedure was done on each subject during one of the two stimulation
208 sessions. Motor mapping was randomly done before, between or after the two procedures. It consisted in

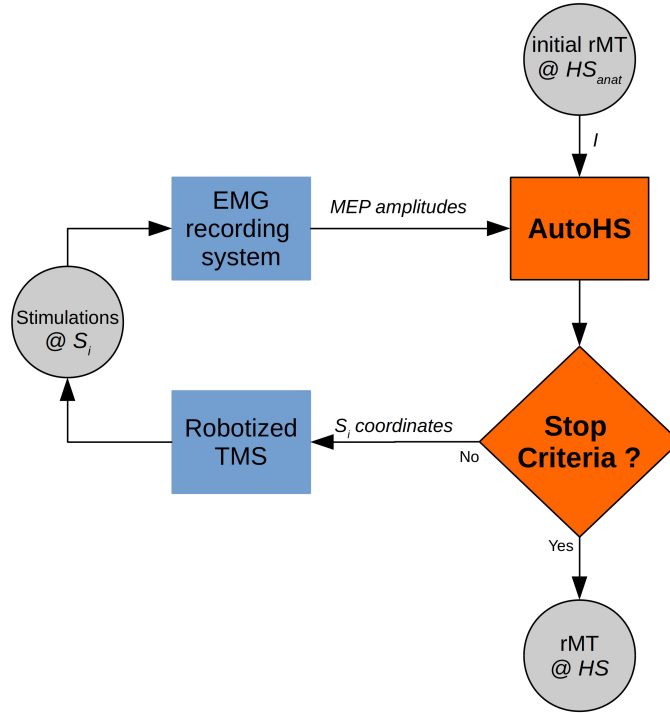


Figure 2: Automatized set-up procedure. The supraliminal stimulation intensity I used for HS hunting is first derived from an initial rMT estimated on HS_{anat} . HS hunting is then iteratively performed by AutoHS, in closed loop with the robotized TMS and the EMG recording systems. Once one of the stop criteria has been satisfied, the model settles the TMS coil over the estimated HS where the actual rMT is assessed.

209 the recording of ten MEPs on each point of the $7*7$ stimulation grid using the robotized system. If the
 210 stimulation failed to evoke a consistent MEP ($> 50 \mu V$) in three consecutive trials, the coil was moved on
 211 to the next site. The stimulation intensity was set to 120 % of the lowest rMT found (by either mSUP or
 212 aSUP) for the corresponding subject.

213 2.2.7. TMS parameters

214 TMS was delivered by a butterfly coil ($2*75$ mm) MagPro Cool B65-RO (MagVenture A/S, Denmark)
 215 plugged into a MagPro X100 stimulator system (MagVenture A/S, Denmark). Biphasic pulses were delivered
 216 using a randomized inter-stimuli interval (ISI) between three and five seconds during mSUP, aSUP and motor
 217 mapping. A ten-second ISI was used during the baseline assessment of mSUP and aSUP. The coil position
 218 and orientation with respect to the individual cortical anatomy were controlled using a neuronavigation
 219 system (Localite GmbH, Germany). Every target and entry points were defined to be normal to the scalp
 220 surface. A robotized system (Axilum Robotics, France) was used during aSUP and motor mapping. All
 221 rMTs were assessed automatically using the PEST procedure (Awiszus and Borckardt, 2011) on 30 trials.

222 2.2.8. EMG parameters

223 The electromyographic activity of the first dorsal interosseous muscle of the dominant hand (right) was
224 recorded using EMG electrodes placed in a belly-tendon montage. EMG data were amplified, band-pass fil-
225 tered (50-6000 Hz), and finally sampled at 12 KHz using a Dantec Keypoint portable EMG recording system
226 (Natus Medical Inc., USA). The EMG activity was recorded in a -200ms to +600ms window surrounding
227 stimulation onset.

228 2.3. Data processing

229 2.3.1. Data of interest

230 The following data were investigated for each procedure:

- 231 • the 2D-coordinates of the HS (in x and y) for each session, reported using a doubled spatial resolution
232 grid (3.5 mm between points instead of 7 mm),
- 233 • the HS shift between the first and second session (in mm), defined as the Euclidean distance between
234 the two HS: $\sqrt{\sum_{x,y} (HS_1 - HS_2)^2}$,
- 235 • the rMT (in % of maximal stimulator output),
- 236 • the procedure duration,
- 237 • the mean and standard deviation of the measured baseline.

238 2.3.2. EMG data

239 EMG data were processed using CortExTool, a Matlab toolbox developed in our lab and freely available to
240 the community (Harquel et al., 2016b). Data were first band-pass filtered (50-600 Hz), and trials containing
241 any muscular activity in the pre-stimulus period were rejected. MEPs were then semi-automatically detected,
242 and their peak to peak amplitudes were extracted. Motor maps showing the MEP mean amplitudes on each
243 stimulation point were generated using a spline 2D interpolation between points (seven iterations).

244 2.3.3. Virtual data

245 Virtual data were generated using the real MEP distributions recorded during motor mapping. For each
246 stimulation position S_i , N MEPs were drawn from a Gaussian distribution $N(\mu_{S_i}, \sigma_{S_i}^2)$, where μ_{S_i} and σ_{S_i}
247 corresponded respectively to the mean and standard deviation of the 10 MEPs recorded on S_i during motor
248 mapping. In order to assess the influence of the parametrical form of the real MEP distribution on the

249 HS hunting performance, amplitudes were multiplied by random values drawn from an uniform distribution
 250 $U(1 - \epsilon, 1 + \epsilon)$ where ϵ represented a noise factor. Three noise factors were tested: 0 (no noise), 0.5, and
 251 0.9 (strong noise). High values modified the mean and standard deviation, while significantly increasing the
 252 skewness and kurtosis of the distribution. Each MEP amplitude y_i was thus calculated as follows:

$$\begin{aligned} y'_i &\sim N(\mu_{S_i}, \sigma_{S_i}^2) \\ n_i &\sim U(1 - \epsilon, 1 + \epsilon) \\ y_i &= y'_i \times n_i. \end{aligned}$$

253 2.3.4. Statistics

254 The results were analyzed through Bayesian statistics. Data were processed using JASP software (JASP
 255 Team (2016)), as well as modified scripts from Kruschke (2014) using R language (R Core Team, 2016)
 256 together with the rjags library. Three basic and standard tests were used: the Bayesian tests equivalent
 257 to paired t-tests, repeated measures ANOVAs, and linear regressions. Prior and likelihood functions were
 258 modeled using Gaussian or Cauchy distributions (the normality of processed data was systematically checked
 259 using Shapiro-Wilk tests). Prior distributions for paired comparison between mSUP and aSUP were kept
 260 wide (i.e. uninformative) and centered on 0, as no previous comparison between aSUP and mSUP was ever
 261 done before. Posterior distributions were computed using a Markov Chain Monte Carlo procedure (10,000
 262 iterations). The convergence and length of the chains were systematically inspected (following the method
 263 detailed in Kruschke (2014)). The posteriors were reported in the text using 95% highest density intervals
 264 (HDI_{95}). HDI_{95} indicates the most probable values for a tested parameter. Evidence of observed effects was
 265 provided using Bayesian factors (see Mulder and Wagenmakers (2016) for an extensive review on this topic):
 266 BF_{01} , BF_{10} (which is the multiplicative inverse of BF_{01}), and BF_{incl} denoted the level of evidence of the
 267 null hypothesis, the alternate hypothesis (non-signed difference), and the inclusion of a specific parameter
 268 in a model (ANOVA) respectively. Bayes factors were interpreted following the cut-offs proposed by Jeffreys
 269 (1998) (values between 1 and 3 denoted absence of evidence to anecdotal evidence, values between 3 and 10
 270 denoted moderate evidence, etc.).

271 3. Results

272 All subjects went through the entire experiment without any major problem. The average MRI co-
 273 registration error, as calculated by the neuronavigation software, was 1.97 ± 0.30 mm. Two subjects were

274 excluded from the experimental comparison, as experimenters did not follow the stimulation angle constraint.
275 Results regarding the reliability and reproducibility of AutoHS on virtual data are first described, followed
276 by the experimental comparison between automatized and manual procedures.

277 *3.1. Model validation*

278 AutoHS was tested on virtual data using either 3, 5, 7 or 10 recorded MEPs per stimulation position,
279 and 3 noise factors ($\epsilon = 0, 0.2, 0.9$). 100 virtual motor maps were generated for each subject and parameter
280 set, leading to a total of 20,400 maps. Overall, it appeared that the model found the HS position in a fast
281 and reliable way, while being more reproducible and less prone to noise than global maximum detection
282 procedures.

283 *Model reliability*

284 The model converged to the HS position for all virtual maps and parameter sets after 13.5 ± 3.3 iterations,
285 i.e. stimulation positions (10.7 ± 1.4 for $N = 5$ and $\epsilon = 0$, using the model's default value on noiseless data).
286 Figure 3a and 3b show in detail the proceedings of the model on one representative virtual motor map. As
287 expected, the entropy h rapidly decreased during HS hunting, while the marginal distributions peaked toward
288 their final estimations of HS position, μ_{HS} and σ_{sp} values. The motor mapping data used in this example is
289 plotted in Figure 3c. The estimated MEP maximum ($\mu_{HS} = 1,750 \mu V$) was close to the recorded maximum
290 ($1,689 \mu V$), and the spatial spread of the muscle representation was correctly estimated ($\sigma_{sp} = 8.4$ mm) by
291 the model.

292 *Spatial reproducibility*

293 A comparison between the spatial reproducibility obtained with AutoHS and with the classical HS
294 hunting procedure was performed by computing the spatial spread of HS positioning on 100 virtual motor
295 maps for each subject (Figure 4). The classical HS hunting procedure is usually based on the observed MEP
296 amplitude, and defines the HS as the cortical position where maximal muscle contraction is induced. To
297 simulate such a procedure, virtual data were analyzed using a global maximum detection procedure, which
298 settled the HS on the point showing the absolute maximum MEP mean amplitude over the complete motor
299 maps (49 points). The spatial spread was defined as the mean standard deviation of HS positions in both
300 axes. The center of gravity (COG) of the motor maps was also computed using $x = \sum (x\mu) / \sum \mu$, and
301 $y = \sum (y\mu) / \sum \mu$ as coordinates, with μ being the mean MEP amplitude for each point of the grid.

302 Overall, the HS spatial spread was smaller using AutoHS (2.8 ± 0.8 mm) than the global maximum
303 detection procedure (3.9 ± 1.6 mm), as stated by the main effect of the method ($BF_{incl} = +\text{inf}$, $HDI_{95} =$

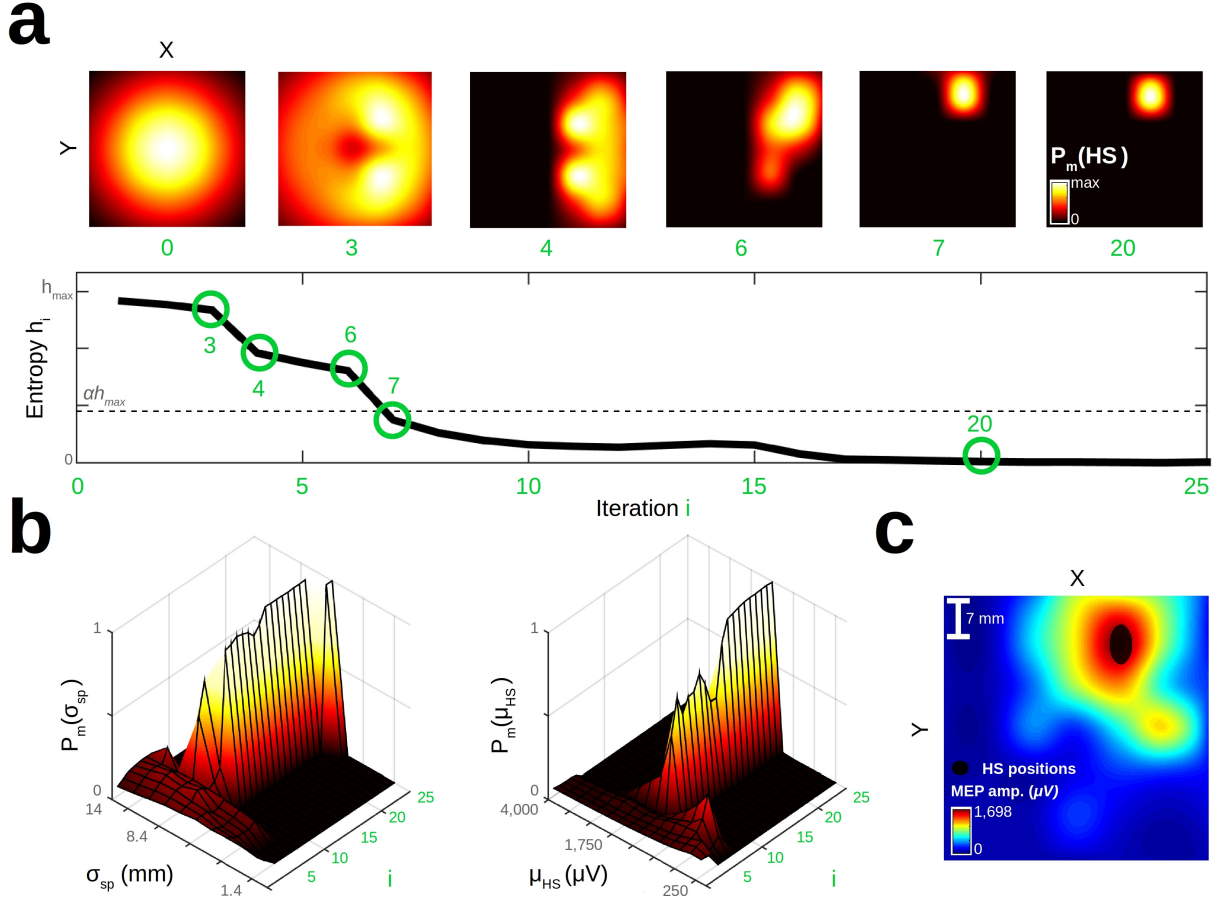


Figure 3: Inferred probability distributions throughout AutoHS, for one virtual motor map of a representative subject (S16). a: (top) Evolution of the marginal distribution $P_m(HS)$ (as defined by Eq.(8)) over time. Iteration 0 represents the prior distribution $P(HS)$. (bottom) Entropy as a function of iterations i . AutoHS settled on the HS position after the 7th stimulation position, inducing an entropy under the defined threshold αh_{max} (see text). b: From left to right, evolution over time of the marginal distributions $P_m(\sigma_{sp})$ and $P_m(\mu_{HS})$ respectively. For this example, AutoHS estimated $\mu_{HS} = 1,750 \mu V$ and $\sigma_{sp} = 8.4 \text{ mm}$. c: Final motor mapping. The black area corresponds to the spatial distribution (1σ ellipse) of the HS positions found during the 100 simulations ($N = 5, \epsilon = 0$).

304 [1.0; 1.4] mm). As expected, the number of recorded MEPs by stimulation points as well as the noise factor
 305 modulated the reproducibility of both methods. HS hunting procedures performed better using more data
 306 (main effect of N , $BF_{incl} = +\text{inf}$) and noise-free data (main effect of ϵ , $BF_{incl} = 4e^{+11}$). It appeared that
 307 the global maximum search procedure was more sensitive to the noise parameter than AutoHS (interaction
 308 effect, $BF_{incl} = 1e^{+7}$), whereas both methods seemed to be equally influenced by the number of MEPs
 309 ($BF_{01} = 5.56$). Figure 4a shows two representative examples of this finding. On the top row, the size of the
 310 dispersion ellipses was modulated by the number of recorded MEPs for both procedures. On the bottom
 311 row, the HSs defined as global MEP maxima tended to spread away from their original position (i.e. without
 312 noise) as the noise factor increased, whereas those inferred by AutoHS remained the same. Figure 4c shows

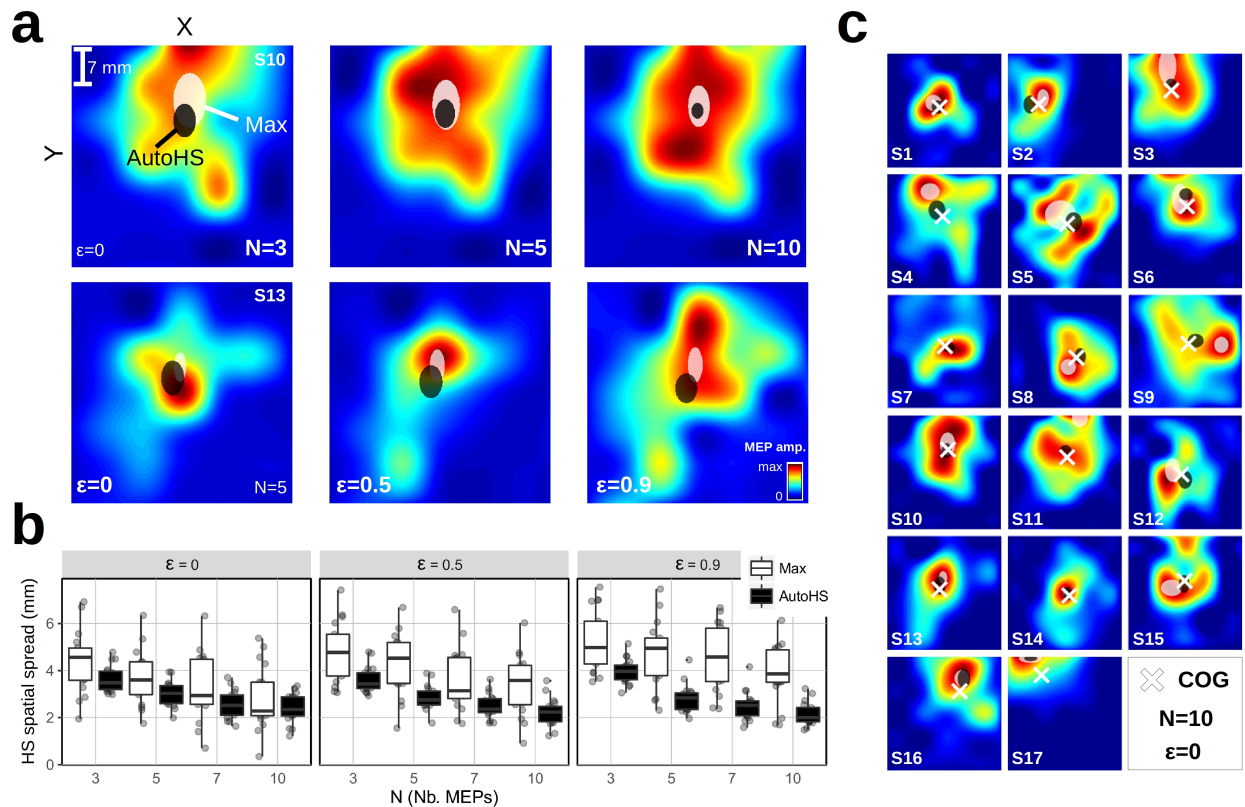


Figure 4: Reproducibility of HS positioning on virtual motor maps, using AutoHS or maximal mean MEP amplitude (Max). a: Results obtained on two representative subjects (S10 and S13). The black and white areas represent the spatial distribution (1σ ellipse) of the HS found by AutoHS and Max procedures for 100 simulations respectively. The distributions are superimposed on motor maps showing the mean MEP amplitude on each point. The top and bottom rows show the influence of N (number of recorded MEPs per stimulation site) and ϵ (noise factor) parameters on the generated motor maps respectively. b: Group result showing the mean HS spatial spread (size of the spatial distribution, see text) observed using AutoHS (black bars) and Max (white bars) procedures for 100 simulations. Data are grouped in X-axis by N and ϵ parameters. c: Spatial distribution of the HS found by AutoHS (black) and Max (white) for all subjects, using 10 noise-free MEPs per point. The center of gravity (COG) is represented by a white cross.

313 the dispersion of HS positions found by global maximum detection procedure and AutoHS, together with
 314 the COG, for all subjects using 10 noiseless MEPs per point ($N = 10$ and $\epsilon = 0$).

315 3.2. Experimental comparison between automatized and manual procedures

316 HS shift

317 Figure 5a shows all the HS positions inferred by both methods on all subjects and sessions, superimposed
 318 on corresponding motor maps. The mean HS shifts were 10.1 ± 6.7 mm for mSUP and 8.2 ± 5.4 mm for
 319 aSUP (Figure 5b). The paired comparison of these two distributions failed to draw any conclusion regarding
 320 their difference ($BF_{10} = 0.4$, $BF_{01} = 2.4$).

321 The average distributions of MEP amplitude surrounding HS were computed for each procedure by
 322 averaging the normalized motor maps (i.e. by dividing each point of the maps by their maximum) centered

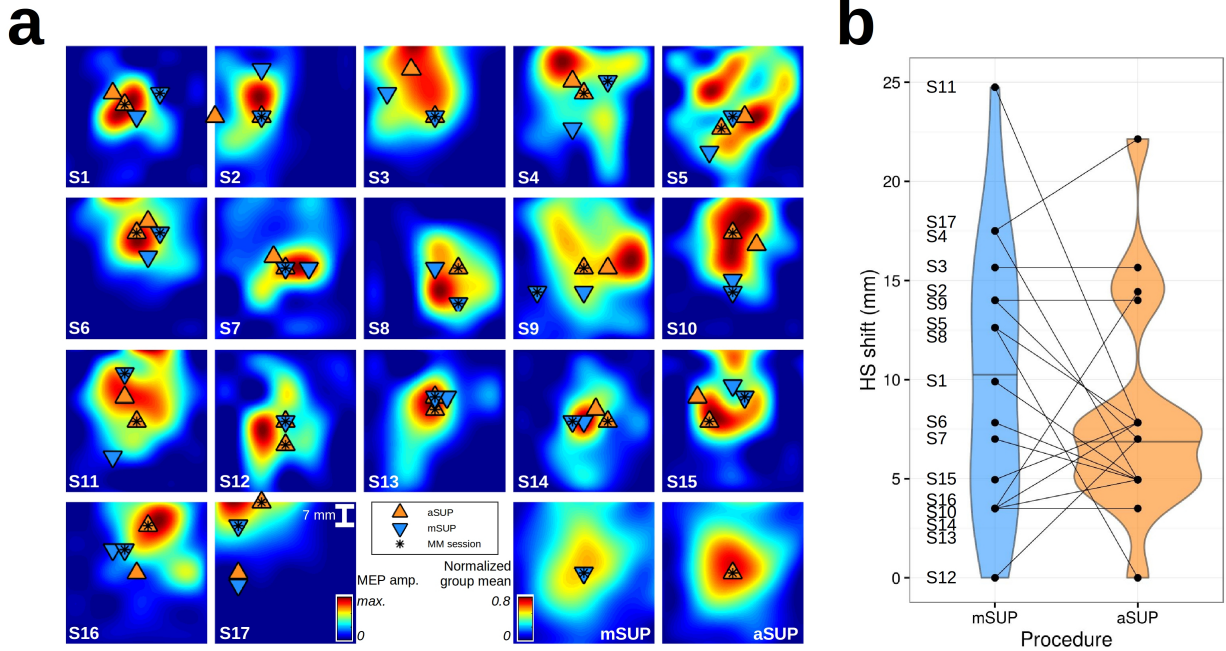


Figure 5: Experimental comparison of mSUP and aSUP regarding the reproducibility of HS positioning. a: HS positions assessed by mSUP (blue) and aSUP (orange) for all subjects and sessions. The positions are superimposed on motor maps showing the mean MEP amplitude on each point. The black stars indicate positions inferred within the same session as motor mapping (MM session). The two supplementary maps (bottom right) represent the average distributions of MEP amplitude surrounding HS inferred by aSUP (left) and mSUP (right). b: HS shift (Euclidean distance between HS found in the two sessions) as a function of procedure. mSUP and aSUP distributions are colored in blue and orange respectively. Pair-wise comparisons are highlighted using segments.

323 on the HS inferred within the same session. The average maps were consequently scaled between 0, no MEP
 324 activity found in any subject, and 1, maximum MEP activity found in all subjects (Figure 5a). aSUP tended
 325 to define HS in the center of a 2D Gaussian shape peaking at 0.71, whereas the HS map inferred by mSUP
 326 was more blurry and spread out towards the anterior direction, leading to a smaller peak value of 0.55.

327 *rMT*

328 Figure 6a presents the results regarding rMTs assessed from mSUP and aSUP, for all subjects and
 329 sessions. The Bayesian repeated measure ANOVA indicated that rMTs were moderately similar between
 330 procedures ($BF_{01} = 3.31$). The mean observed rMT was $46.4 \pm 7.5\%$ for mSUP and $45.7 \pm 7.1\%$ for
 331 aSUP. rMTs were strongly correlated between the two sessions for both methods (Figure 6c). However,
 332 the most probable values of the correlation and its evidence were higher for aSUP ($HDI_{95}(\rho) = [0.73; 0.97]$,
 333 $BF_{10} = 6e^4$) than for mSUP ($HDI_{95}(\rho) = [0.43; 0.91]$, $BF_{10} = 185$). A Bayesian ANOVA on rMTs assessed
 334 during mSUP using experimenters as fixed factor, and subjects and sessions as noise factors, provided
 335 moderate evidence that the experimenters did not influence rMT ($BF_{01} = 3.45$).

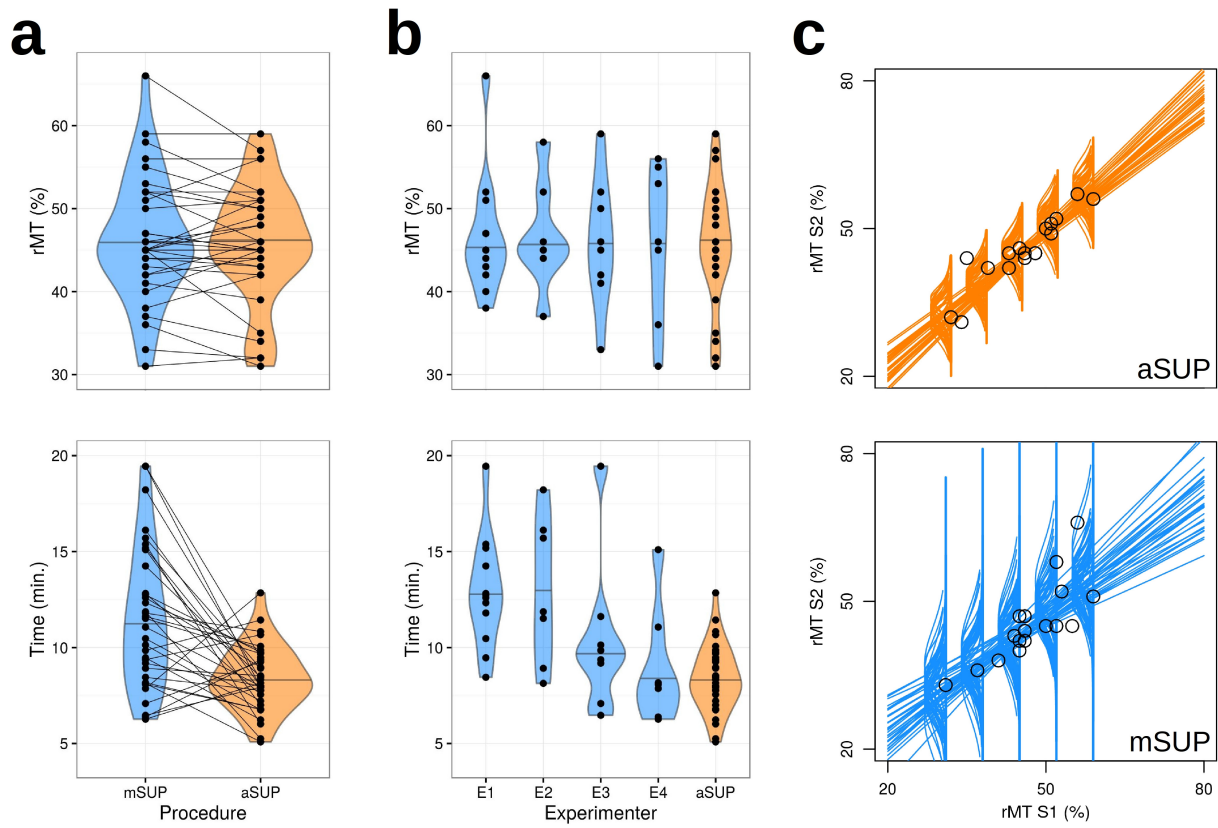


Figure 6: Experimental comparison of mSUP and aSUP performances based on rMTs and procedure durations. mSUP and aSUP distributions are colored in blue and orange respectively. Paired-wise comparisons are highlighted using segments. a: distributions of inferred rMT (top) and procedure durations (bottom) using mSUP and aSUP, for all subjects and sessions. b: distributions of mSUP values for each of the four experimenters compared to the aSUP values (top: rMT, bottom: procedure duration). c: inter session correlation between rMTs for aSUP (top) and mSUP (bottom), where a sample of credible regression lines are plotted.

336 *Estimated duration*

337 Figure 6a shows the comparison between the duration of mSUP and aSUP, for all subjects and sessions.
 338 The theoretical duration of aSUP was simulated by considering AutoHS as fully implemented in the TMS
 339 acquisition loop (Figure 3), using an ISI of 5 seconds and an interval of 3 seconds between stimulation
 340 positions, compensating for the robotized arm movement. Both durations included the rMT assessment
 341 time and thus represented the time of the whole set-up procedures, from the first TMS pulse to the final
 342 rMT outcome. It appeared that aSUP lasted shorter than mSUP ($HDI_{95} = [1.6; 4.6]$ min, $BF_{10} = 273$).
 343 On average, mSUP lasted 11.5 ± 3.7 min while aSUP lasted 8.3 ± 1.7 min. A Bayesian ANOVA was run on
 344 the mSUP duration using experimenters as fixed factor, and subjects and sessions as random factors. No
 345 conclusion could be drawn regarding the influence of the experimenters on the procedure time ($BF_{incl} =$
 346 1.16 , $BF_{01} = 0.87$).

347 *Baseline measurements*

348 The baseline means were $999 \pm 848 \mu V$ for mSUP and $852 \pm 609 \mu V$ for aSUP. There was a moderate
349 evidence that they did not differ between methods ($BF_{01} = 3.6$ for the method effect). The average baseline
350 standard deviations were $526 \pm 363 \mu V$ for mSUP and $462 \pm 369 \mu V$ for aSUP, and did not differ between
351 methods ($BF_{01} = 4.6$).

352 **4. Discussion**

353 This work provides the first proof of concept for a practical and fully automatized set-up procedure
354 dedicated to TMS protocols. The core element of this procedure is a Bayesian model, AutoHS, which guides
355 the HS hunting. Results of both simulations and experimental comparison against classical methodologies are
356 promising. The automatized procedure appears to be at least as reliable as the manual one, while being more
357 reproducible and significantly shorter than the necessary processing time of this step. Moreover, this work
358 challenges the classical hotspot definition, and supports the need for future developments, optimizations,
359 and extensions of the model to other experimental fields in TMS.

360 *4.1. Robustness of the model*

361 The hypothesis regarding the relationship between recorded MEP amplitudes and distance to the HS
362 may be one of the most influential factor on model performance. It is based on the assumption that muscle
363 representations are centered symmetrically around the HS. Even though this hypothesis appeared to be
364 violated with varying degrees in most of the subjects, it did not prevent the model to systematically converge
365 towards reliable and reproducible solutions. However, assuming that targeted muscles are restricted to uni-
366 modal representations may be erroneous for any kind of HS hunting procedure. The functional organization
367 of the primary motor cortex is more complex than a successive arrangement of muscle representations along
368 the central sulcus (Schieber, 2001). While S1 somatotopy has a discrete and segregated layout of body
369 part representations, M1 in contrast displays a more integrated and overlapping functional organization.
370 Recent invasive stimulation studies on both animals and humans clearly identified representations of several
371 synergies and multijoint movements over the motor cortex (Graziano and Aflalo, 2007 ; Desmurget et al.,
372 2014 ; Giszter, 2015). The conception of M1 as a simple body plan is shifting to a more complex picture that
373 includes action representations (Graziano, 2016). Our motor mapping data (see S1, S4, S5, S9 and S10), as
374 well as many examples in the literature, suggest that the FDI representation is far from being uni-modal in
375 some subjects (see the motor or MT maps shown in Gugino et al. (2001) ; Neggers et al. (2004) ; Sparing

376 et al. (2008) ; Meesen et al. (2011) ; van de Ruit et al. (2015) ; Meincke et al. (2016)). Additionally, significant
377 muscular contractions can also be induced when stimulating pre-motor areas (Ahdab et al., 2016), which are
378 sometimes included in the most anterior part of the stimulation space, depending on the gyri configuration
379 (see S3, S6, S11 and S15). Despite the fact that the spatial spread of the electrical field induced by TMS
380 might be limiting for revealing such complex multiple representations in most of subjects, choosing multi-
381 modal distributions for muscle representations may optimize the method for the rest of them. Testing our
382 procedure with more focal coils could also allow to better observe and take into account this phenomenon.

383 The assumption of Gaussianity regarding MEP distributions has been extensively tested on virtual data.
384 The model appeared to be very robust to its violation, i.e. when MEP distributions were not Gaussian.
385 As shown in Figure 4a and b, the reproducibility of the method stayed unaffected by increasing noise
386 factors, contrary to the global maximum search procedure. As a trade-off, the convergence speed was
387 however reduced from 11 (perfect Gaussian distributions) to 17 iterations (noisy distributions) on average.
388 The prior regarding the HS position had little influence on model performance. By choosing a large value
389 for σ_{prior} (14 mm), the prior was kept uninformative so that its influence was minimized compared to
390 the iterative exploration process. Recorded data supported this choice, as only one subject (S14) showed
391 maximal contractions exactly on the anatomical prior for HS position. For these particular cases, choosing a
392 lower value for σ_{prior} could then increase the convergence speed (about 3 iterations for $\sigma_{prior} = 4$ mm). On
393 average, choosing a wider or a narrower prior distribution would slightly decrease or increase the convergence
394 speed respectively, depending on the distance between the real and anatomical HS, i.e. depending on the
395 goodness of the prior.

396 Variable domains should always cover the most probable physiological values regarding MEP amplitudes,
397 or spatial spreads of muscle representations. Choosing domains larger than the proposed defaults would
398 enable the model to cover more particular cases. However, recording maximum MEP amplitudes higher than
399 $4 \mu V$, or spatial muscle representations larger than 14 mm, are highly improbable using the proposed stimu-
400 lation intensity. Choosing more precise domains, i.e. using smaller steps between values, would theoretically
401 make the probabilistic inference more precise, while consequently increasing computing time significantly.
402 Finally, the values defining the stop criteria are always representative of the trade-off between procedure
403 precision and duration. Higher values for the entropy thresholds (α and β) would allow decreasing procedure
404 time, as they would be reached faster, while lowering the reproducibility of the calculation (see the example
405 depicted in Figure 3a).

406 4.2. Redefining the HS

407 By developing AutoHS, we slightly revisited the interpretation of the most commonly used HS definition.
408 Theoretically, the HS is the site where TMS induces maximal contractions over a targeted muscle. Most
409 TMS experimenters generally assess HS by finding the position of the global maximum within the stimulation
410 space, by computing the mean of several trials for each site. In contrast, AutoHS looks for the *probabilistic*
411 position of this maximum. By fully taking inter-trial variability into account, probabilistic methods are more
412 reliable than global maximum search procedures and are less prone to outliers. This is especially important
413 given the high trial-to-trial variability of MEP amplitude and our results on virtual data strongly support
414 the beneficial contribution of the probabilistic approach to HS determination. We found that the average
415 HS shift was significantly reduced between virtual sessions with AutoHS, especially when data were noisy.
416 Interestingly, our procedure led to a good solution between the global maximum of the motor maps and its
417 center of gravity. Like the COG, it tended to position the HS in the center of large muscle representations
418 (see for example Figure 4c, subjects S3, S4, S9, S11), while it rather converged to global maximum position
419 for narrower motor maps (see S16 and S17).

420 The optimization in HS positioning had a direct effect regarding the reproducibility of outcomes during
421 the experimental comparison with manual methods. The automatized set-up procedure showed improved
422 inter-session reproducibility regarding the measured rMT. Experimental results also confirmed that it was
423 more reliable than the manual procedure in finding a position inducing maximal contractions. The aver-
424 age motor maps presented in the bottom right part of Figure 5a are especially meaningful. Overall, the
425 automatized method sets the HS over the maximum contraction point at a higher rate than the manual
426 one. However, our work failed to bring strong evidence for an improvement of the measured outcomes reli-
427 ability, i.e. smaller rMT and baseline variability, due to a high inter-subject variability between procedure
428 performance. Three non-exclusive hypotheses can be posited to explain the lack of result regarding relia-
429 bility. First, as suggested by the small BF values, further data have to be acquired in the future in order
430 to accumulate more evidence in favor of one or another hypothesis. Second, the current neuronavigation
431 system precision, about 3 mm when adding the registration error and the camera precision (1 mm), and
432 TMS spatial resolution might not have the ability to detect fine differences in HS shift induced by AutoHS
433 compared to classical approaches. Using smaller coils and more precise camera might be two solutions for
434 solving these issues respectively. Finally, our model is still not fully optimized regarding its hypotheses
435 and stop criteria. Developing better and more adaptable priors about MEP spatial distribution, as well
436 as lowering the thresholds for stop criteria could improve the reliability of HS positioning and measured

437 outcomes, while slightly increasing the number of needed stimulation targets, as a trade-off (see 4.1).

438 4.3. Future developments

439 This initial study paves the way for future optimizations and developments of AutoHS, by reconsidering
440 some of the hypotheses of the model, including angle estimation in its process, and extending its principle
441 to other experimental fields.

442 First, the subject anatomy and gyral geometry should be better taken into account in the stimulation
443 space. The model should first include the scalp-to-cortex distance and adapt the stimulation intensity to it
444 (Stokes et al., 2005), as it may vary within the stimulation space. Second, even if the square grid used in this
445 work covered most of the precentral gyrus, the exploration space would be optimized using a non-cartesian
446 stimulation grid exactly following the gyrus shape towards the X-axis. A recent study showed that TMS
447 could better discriminate between muscles when following the gyral geometry compared to following its
448 main direction (Raffin et al., 2015). Second, the parametrical form of the distribution of MEP amplitudes
449 knowing the positions of HS and the stimulation point ($P(\mu_i | A)$) is simplistic and non-optimal for several
450 subjects, especially for those presenting a bi-modal distribution (see above). Less constrained parametrical
451 forms could be tested. For instance, introducing covariance terms in the 2D Gaussian would allow capturing
452 decrease of MEP amplitudes not geometrically aligned with the grid; using Gaussian mixtures would allow
453 capturing multi-modality; etc.

454 Second, the model should estimate the optimized stimulation angle within its process. As shown in
455 previous studies, the stimulation angle may have a strong influence over the inferred rMT on some subjects
456 (Richter et al., 2013). Using a single stimulation angle (perpendicular to the precentral gyrus) might be
457 limiting here, even if it is theoretically supposed to be the most adapted. Two factors might at least
458 influence the optimal stimulation angle within an actual experiment: errors in the MRI registration and
459 complex modulations of the induced electrical field geometry by neuro-anatomical properties (Thielscher
460 et al., 2011 ; Janssen et al., 2015). In this study, two subjects were excluded of the experimental comparison
461 as experimenters did not follow the angle constraint (disparities of 30 and 50°), inducing a rMT difference of
462 $\pm 10\%$ between the two procedures (opposite in direction). It appeared then that the pre-defined stimulation
463 angle was not optimal in at least one case. In future developments of the method, the stimulation angle
464 should become a variable of the model and be estimated during HS hunting.

465 Finally, the core principle of the model can be applied beyond the specific HS hunting problem, *i.e.*
466 in any experimental procedure aiming at finding a cortical target optimized using TMS readouts. More

467 specifically, it can be adapted to find the probabilistic origin of any a priori known distribution of TMS-
468 induced readouts over a stimulation space. In principle, the TMS readouts can be either behavioral or
469 neurophysiological. For example, the model could be modified for developing a phosphene tresholding
470 procedure over the occipital cortex (Dugué et al., 2011 ; Herring et al., 2015). It could also be turned into
471 a functional area hunting procedure, by estimating the stimulated cortical target best able to modulate the
472 performance of a specific cognitive task. Finally, the model could also be applied in concurrence with other
473 brain imaging technique, like electroencephalography (EEG). Under this condition, it would allow to find
474 stimulation areas optimizing the emergence of any EEG components, such as evoked potentials or induced
475 oscillations, in order to help the characterization of specific outcomes or biomarkers in various clinical or
476 fundamental issues (see Farzan et al. (2016) for a recent review). Such procedure would also be especially
477 useful in future closed-loop approaches combining TMS and electrophysiology (Bergmann et al., 2016), that
478 aim at adapting the stimulation parameters based on readouts in real time.

479 **5. Authors contribution**

480 S.H., J.D., E.R., and A.C. designed research. S.H., E.R., B.P., G.I., C.M. and A.C. performed research.
481 S.H. and B.P. analysed data. S.H., J.D., E.R., O.D. and A.C. wrote the paper.

482 **6. Acknowledgments**

483 This work was funded by the Pôle Grenoble Cognition grant “PGC-2014” and the Agence Nationale
484 pour la Recherche grant “ANR-15-CE37-0015-02”. Data were acquired on a platform of France Life Imaging
485 network partly funded by the grant “ANR-11-INBS-0006”. The authors declare no conflict of interest.

486 **7. Appendix**

The derivation leading to Eq. (7) used during Bayesian inference is :

$$\begin{aligned}
& P(HS \ \mu_{HS} \ \sigma_{sp} \mid S_{1:T} \ \mu_{1:T}) \\
&= \frac{P(HS \ \mu_{HS} \ \sigma_{sp} \ S_{1:T} \ \mu_{1:T})}{P(S_{1:T} \ \mu_{1:T})} && \text{[Bayes theorem]} \\
&= \frac{1}{Z_1} P(HS \ \mu_{HS} \ \sigma_{sp} \ S_{1:T} \ \mu_{1:T}) && [P(S_{1:T} \ \mu_{1:T}) = Z_1 \text{ (constant)}] \\
&= \frac{1}{Z_1} P(HS) P(\mu_{HS}) P(\sigma_{sp}) \prod_{i=1}^T P(S_i) \prod_{i=1}^T P(\mu_i \mid HS \ \mu_{HS} \ \sigma_{sp} \ S_i) && \text{[by definition of the joint]} \\
&= \frac{1}{Z_1 Z_2} P(HS) \prod_{i=1}^T P(S_i) \prod_{i=1}^T P(\mu_i \mid HS \ \mu_{HS} \ \sigma_{sp} \ S_i) && [P(\mu_{HS})P(\sigma_{sp}) = Z_2 \text{ (uniforms)}] \\
&= \frac{1}{Z_1 Z_2} P(HS) \prod_{i=1}^T P(\mu_i \mid HS \ \mu_{HS} \ \sigma_{sp} \ S_i) && [P(S_i) = 1 \text{ (Dirac)}] \\
&\propto P(HS) \prod_{i=1}^T P(\mu_i \mid HS \ \mu_{HS} \ \sigma_{sp} \ S_i) && \square \\
&\propto P(HS) \prod_{i=1}^T P(\mu_i \mid A) && (14)
\end{aligned}$$

487 recalling that A is the conjunction of variables HS , μ_{HS} , σ_{sp} and S_i .

488 **8. References**

- 489 Ahdab, R., Ayache, S. S., Brugières, P., Farhat, W. H., Lefaucheur, J.-P., Mar. 2016. The Hand Motor Hotspot is not Always
490 Located in the Hand Knob: A Neuronavigated Transcranial Magnetic Stimulation Study. *Brain Topography*, 1–8.
- 491 Awiszus, F., 2003. TMS and threshold hunting. *Supplements to Clinical Neurophysiology* 56, 13–23.
- 492 Awiszus, F., Borckardt, J., 2011. TMS motor threshold assessment tool (MTAT 2.0).
- 493 Baek, J., Lesmes, L. A., Lu, Z.-L., Aug. 2016. qPR: An adaptive partial-report procedure based on Bayesian inference. *Journal*
494 *of Vision* 16 (10), 25.
- 495 Barker, A. T., Jalinous, R., Freeston, I. L., May 1985. Non-invasive magnetic stimulation of human motor cortex. *The Lancet*
496 325 (8437), 1106–1107.
- 497 Bergmann, T. O., Karabanov, A., Hartwigsen, G., Thielscher, A., Siebner, H. R., 2016. Combining non-invasive transcranial
498 brain stimulation with neuroimaging and electrophysiology: Current approaches and future perspectives. *NeuroImage*.
499 URL <http://www.sciencedirect.com/science/article/pii/S1053811916001191>
- 500 Bessière, P., Mazer, E., Ahuactzin, J. M., Mekhnacha, K., 2013. *Bayesian Programming*. CRC Press, Boca Raton, Florida.
- 501 Bessière, P., Lebeltel, O., 2008. Basic Concepts of Bayesian Programming. In: Bessière, P., Laugier, C., Siegwart, R. (Eds.),
502 Probabilistic Reasoning and Decision Making in Sensory-Motor Systems. No. 46 in Springer Tracts in Advanced Robotics.
503 Springer Berlin Heidelberg, pp. 19–48, doi: 10.1007/978-3-540-79007-5_2.

504 Bestmann, S., Feredoes, E., Aug. 2013. Combined neurostimulation and neuroimaging in cognitive neuroscience: past, present,
505 and future: Combined neurostimulation and neuroimaging. *Annals of the New York Academy of Sciences* 1296 (1), 11–30.

506 Bortoletto, M., Veniero, D., Thut, G., Miniussi, C., Feb. 2015. The contribution of TMS–EEG coregistration in the exploration
507 of the human cortical connectome. *Neuroscience & Biobehavioral Reviews* 49, 114–124.

508 Cincotta, M., Giovannelli, F., Borgheresi, A., Balestrieri, F., Toscani, L., Zaccara, G., Carducci, F., Viggiano, M. P., Rossi,
509 S., Apr. 2010. Optically tracked neuronavigation increases the stability of hand-held focal coil positioning: Evidence from
510 “transcranial” magnetic stimulation-induced electrical field measurements. *Brain Stimulation* 3 (2), 119–123.

511 Desmurget, M., Richard, N., Harquel, S., Baraduc, P., Szathmari, A., Mottolese, C., Sirigu, A., Apr. 2014. Neural representa-
512 tions of ethologically relevant hand/mouth synergies in the human precentral gyrus. *Proceedings of the National Academy*
513 *of Sciences* 111 (15), 5718–5722.

514 Dugué, L., Marque, P., VanRullen, R., Aug. 2011. The Phase of Ongoing Oscillations Mediates the Causal Relation between
515 Brain Excitation and Visual Perception. *The Journal of Neuroscience* 31 (33), 11889–11893.

516 Farzan, F., Vernet, M., Shafi, M. M. D., Rotenberg, A., Daskalakis, Z. J., Pascual-Leone, A., Sep. 2016. Characterizing and
517 Modulating Brain Circuitry through Transcranial Magnetic Stimulation Combined with Electroencephalography. *Frontiers*
518 *in Neural Circuits* 10.
519 URL <http://journal.frontiersin.org/Article/10.3389/fncir.2016.00073/abstract>

520 Finke, M., Fadini, T., Kantelhardt, S., Giese, A., Matthaus, L., Schweikard, A., 2008. Brain-mapping using robotized TMS.
521 In: *Engineering in Medicine and Biology Society, 2008. EMBS 2008. 30th Annual International Conference of the IEEE*. pp.
522 3929–3932.

523 Ginhoux, R., Renaud, P., Zorn, L., Goffin, L., Bayle, B., Foucher, J., Lamy, J., Armspach, J. P., de Mathelin, M., 2013. A
524 custom robot for transcranial magnetic stimulation: first assessment on healthy subjects. In: *2013 35th Annual International*
525 *Conference of the IEEE Engineering in Medicine and Biology Society (EMBC)*. IEEE, pp. 5352–5355.

526 Giszter, S. F., Aug. 2015. Motor primitives — new data and future questions. *Current Opinion in Neurobiology* 33, 156–165.

527 Graziano, M. S. A., Feb. 2016. Ethological Action Maps: A Paradigm Shift for the Motor Cortex. *Trends in Cognitive Sciences*
528 20 (2), 121–132.

529 Graziano, M. S. A., Afalo, T. N., Oct. 2007. Mapping Behavioral Repertoire onto the Cortex. *Neuron* 56 (2), 239–251.

530 Gugino, L. D., Rafael Romero, J., Aglio, L., Titone, D., Ramirez, M., Pascual-Leone, A., Grimson, E., Weisenfeld, N., Kikinis,
531 R., Shenton, M.-E., Oct. 2001. Transcranial magnetic stimulation coregistered with MRI: a comparison of a guided versus
532 blind stimulation technique and its effect on evoked compound muscle action potentials. *Clinical Neurophysiology* 112 (10),
533 1781–1792.

534 Hallett, M., 2000. Transcranial magnetic stimulation and the human brain. *Nature* 406 (6792), 147–150.

535 Harquel, S., Bacle, T., Beynel, L., Marendaz, C., Chauvin, A., David, O., May 2016a. Mapping dynamical properties of cortical
536 microcircuits using robotized TMS and EEG: Towards functional cytoarchitectonics. *NeuroImage* 135, 115–124.

537 Harquel, S., Beynel, L., Guyader, N., Marendaz, C., David, O., Chauvin, A., Oct. 2016b. CortExTool: a toolbox for processing
538 motor cortical excitability measurements by transcranial magnetic stimulation.
539 URL <https://hal.archives-ouvertes.fr/hal-01390016/document>

540 Herbsman, T., Forster, L., Molnar, C., Dougherty, R., Christie, D., Koola, J., Ramsey, D., Morgan, P. S., Bohning, D. E.,
541 George, M. S., Nahas, Z., Jul. 2009. Motor Threshold in Transcranial Magnetic Stimulation: The Impact of White Matter
542 Fiber Orientation and Skull-to-Cortex Distance. *Human brain mapping* 30 (7), 2044–2055.

543 Herring, J. D., Thut, G., Jensen, O., Bergmann, T. O., Oct. 2015. Attention Modulates TMS-Locked Alpha Oscillations in the
544 Visual Cortex. *The Journal of Neuroscience* 35 (43), 14435–14447.

545 Herwig, U., Schönfeldt-Lecuona, C., Wunderlich, A. P., von Tiesenhäusen, C., Thielscher, A., Walter, H., Spitzer, M., Nov.
546 2001. The navigation of transcranial magnetic stimulation. *Psychiatry Research: Neuroimaging* 108 (2), 123–131.

547 Janssen, A. M., Oostendorp, T. F., Stegeman, D. F., May 2015. The coil orientation dependency of the electric field induced
548 by TMS for M1 and other brain areas. *Journal of NeuroEngineering and Rehabilitation* 12.

549 Jeffreys, H., Aug. 1998. *The Theory of Probability*. OUP Oxford.

550 Julkunen, P., Säisänen, L., Danner, N., Niskanen, E., Hukkanen, T., Mervaala, E., Könönen, M., Feb. 2009. Comparison
551 of navigated and non-navigated transcranial magnetic stimulation for motor cortex mapping, motor threshold and motor
552 evoked potentials. *NeuroImage* 44 (3), 790–795.

553 Jung, N. H., Delvendahl, I., Kuhnke, N. G., Hauschke, D., Stolle, S., Mall, V., Apr. 2010. Navigated transcranial magnetic
554 stimulation does not decrease the variability of motor-evoked potentials. *Brain Stimulation* 3 (2), 87–94.

555 Kantelhardt, S. R., Fadini, T., Finke, M., Kallenberg, K., Siemerikus, J., Bockermann, V., Matthaues, L., Paulus, W.,
556 Schweikard, A., Rohde, V., Giese, A., Nov. 2009. Robot-assisted image-guided transcranial magnetic stimulation for so-
557 matotopic mapping of the motor cortex: a clinical pilot study. *Acta Neurochirurgica* 152 (2), 333–343.

558 Kruschke, J., Nov. 2014. *Doing Bayesian Data Analysis: A Tutorial with R, JAGS, and Stan*. Academic Press.

559 Lefaucheur, J.-P., André-Obadia, N., Antal, A., Ayache, S. S., Baeken, C., Benninger, D. H., Cantello, R. M., Cincotta,
560 M., de Carvalho, M., De Ridder, D., Devanne, H., Di Lazzaro, V., Filipović, S. R., Hummel, F. C., Jääskeläinen, S. K.,
561 Kimiskidis, V. K., Koch, G., Langguth, B., Nyffeler, T., Oliviero, A., Padberg, F., Poulet, E., Rossi, S., Rossini, P. M.,
562 Rothwell, J. C., Schönfeldt-Lecuona, C., Siebner, H. R., Slotema, C. W., Stagg, C. J., Valls-Sole, J., Ziemann, U., Paulus,
563 W., Garcia-Larrea, L., Nov. 2014. Evidence-based guidelines on the therapeutic use of repetitive transcranial magnetic
564 stimulation (rTMS). *Clinical Neurophysiology* 125 (11), 2150–2206.

565 Lefaucheur, J.-P., Picht, T., Apr. 2016. The value of preoperative functional cortical mapping using navigated TMS. *Neuro-*
566 *physiologie Clinique/Clinical Neurophysiology* 46 (2), 125–133.

567 Meesen, R. L., Cuypers, K., Rothwell, J. C., Swinnen, S. P., Levin, O., Jun. 2011. The effect of long-term TENS on persistent
568 neuroplastic changes in the human cerebral cortex. *Human Brain Mapping* 32 (6), 872–882.

569 Meincke, J., Hewitt, M., Batsikadze, G., Liebetanz, D., Jan. 2016. Automated TMS hotspot-hunting using a closed loop
570 threshold-based algorithm. *NeuroImage* 124, Part A, 509–517.

571 Mulder, J., Wagenmakers, E.-J., Jun. 2016. Editors’ introduction to the special issue “Bayes factors for testing hypotheses in
572 psychological research: Practical relevance and new developments”. *Journal of Mathematical Psychology* 72, 1–5.

573 Neggers, S. F. W., Langerak, T. R., Schutter, D. J. L. G., Mandl, R. C. W., Ramsey, N. F., Lemmens, P. J. J., Postma, A.,
574 Apr. 2004. A stereotactic method for image-guided transcranial magnetic stimulation validated with fMRI and motor-evoked
575 potentials. *NeuroImage* 21 (4), 1805–1817.

576 R Core Team, 2016. *R: A Language and Environment for Statistical Computing*. R Foundation for Statistical Computing,
577 Vienna, Austria.

578 URL <https://www.R-project.org>

579 Raffin, E., Pellegrino, G., Di Lazzaro, V., Thielscher, A., Siebner, H. R., Oct. 2015. Bringing transcranial mapping into shape:
580 Sulcus-aligned mapping captures motor somatotopy in human primary motor hand area. *NeuroImage* 120, 164–175.

581 Ragazzoni, A., Pirulli, C., Veniero, D., Feurra, M., Cincotta, M., Giovannelli, F., Chiaramonti, R., Lino, M., Rossi, S., Miniussi,

582 C., 2013. Vegetative versus minimally conscious states: a study using TMS-EEG, sensory and event-related potentials. PLOS
583 ONE 8 (2), e57069.

584 Richter, L., Neumann, G., Oung, S., Schweikard, A., Trillenber, P., Apr. 2013. Optimal Coil Orientation for Transcranial
585 Magnetic Stimulation. PLOS ONE 8 (4), e60358.

586 Rogasch, N. C., Fitzgerald, P. B., Jul. 2013. Assessing cortical network properties using TMS-EEG. Human Brain Mapping
587 34 (7), 1652–1669.

588 Rossi, S., Hallett, M., Rossini, P. M., Pascual-Leone, A., Dec. 2009. Safety, ethical considerations, and application guidelines for
589 the use of transcranial magnetic stimulation in clinical practice and research. Clinical Neurophysiology 120 (12), 2008–2039.

590 Rossini, P. M., Barker, A. T., Berardelli, A., Caramia, M. D., Caruso, G., Cracco, R. Q., Dimitrijević, M. R., Hallett, M.,
591 Katayama, Y., Lücking, C. H., Aug. 1994. Non-invasive electrical and magnetic stimulation of the brain, spinal cord and
592 roots: basic principles and procedures for routine clinical application. Report of an IFCN committee. Electroencephalography
593 and Clinical Neurophysiology 91 (2), 79–92.

594 Schieber, M. H., Nov. 2001. Constraints on Somatotopic Organization in the Primary Motor Cortex. Journal of Neurophysiology
595 86 (5), 2125–2143.

596 Sollmann, N., Hauck, T., Obermüller, T., Hapfelmeier, A., Meyer, B., Ringel, F., Krieg, S. M., 2013. Inter- and intraobserver
597 variability in motor mapping of the hotspot for the abductor pollicis brevis muscle. BMC Neuroscience 14 (1), 94.

598 Sparing, R., Buelte, D., Meister, I. G., Pauš, T., Fink, G. R., Jan. 2008. Transcranial magnetic stimulation and the challenge
599 of coil placement: A comparison of conventional and stereotaxic neuronavigational strategies. Human Brain Mapping 29 (1),
600 82–96.

601 Stokes, M. G., Chambers, C. D., Gould, I. C., Henderson, T. R., Janko, N. E., Allen, N. B., Mattingley, J. B., Dec. 2005.
602 Simple Metric For Scaling Motor Threshold Based on Scalp-Cortex Distance: Application to Studies Using Transcranial
603 Magnetic Stimulation. Journal of Neurophysiology 94 (6), 4520–4527.

604 Thielscher, A., Opitz, A., Windhoff, M., Jan. 2011. Impact of the gyral geometry on the electric field induced by transcranial
605 magnetic stimulation. NeuroImage 54 (1), 234–243.

606 van de Ruit, M., Perenboom, M. J. L., Grey, M. J., 2015. TMS Brain Mapping in Less Than Two Minutes. Brain Stimulation
607 8, 231–239.

608 Wassermann, E., Epstein, C. (Eds.), Nov. 2012. The Oxford handbook of transcranial stimulation. Oxford University Press,
609 Great Clarendon Street, Oxford, OX2 6DP.

610 Wassermann, E. M., Jul. 2002. Variation in the response to transcranial magnetic brain stimulation in the general population.
611 Clinical Neurophysiology 113 (7), 1165–1171.

612 Weiss, C., Nettekoven, C., Rehme, A. K., Neuschmelting, V., Eisenbeis, A., Goldbrunner, R., Grefkes, C., Feb. 2013. Mapping
613 the hand, foot and face representations in the primary motor cortex — Retest reliability of neuronavigated TMS versus
614 functional MRI. NeuroImage 66, 531–542.

615 Yousry, T. A., Schmid, U. D., Alkadhi, H., Schmidt, D., Peraud, A., Buettner, A., Winkler, P., 1997. Localization of the motor
616 hand area to a knob on the precentral gyrus. A new landmark. Brain 120 (1), 141–157.